

Austenite Grain Growth in a Nuclear Pressure Vessel Steel

H. Pous-Romero^a, I. Lonardelli^a, D. Cogswell^b, H. K. D. H. Bhadeshia^a

^a*Department of Materials Science and Metallurgy, University of Cambridge, Cambridge, U.K.*

^b*Rolls-Royce plc, Derby, UK*

Abstract

There is uncertainty on the physical significance of models applied to the coarsening of austenite grains in nuclear pressure vessel steels. As a result, new data are generated and analysed by adapting standard theory to account for the initial austenite grain size generated when the steel becomes fully austenitic, and any growth during heating to the annealing temperature. The experimental data reflect two regimes of isothermal grain coarsening, with grain boundary pinning dominating the kinetics at temperatures below about 940°C. The precipitates responsible for this pinning have been identified using thermodynamics, high-energy X-rays, transmission electron microscopy and microanalysis as aluminium nitrides. The model accounting for all these factors seems to generalise well on unseen data.

Keywords: Austenite grain size, SA508, Aluminium nitride

1. Introduction

There are only a few steels that have been sufficiently tested for approved use in the construction of nuclear pressure vessels, partly because the qualification of such materials requires an enormous amount of time-consuming work. The reactor pressure vessels (RPV) in particular have demanding requirements for tensile strength, toughness and resistance to irradiation embrittlement over the projected service life [1, 2]. One of the popular alloys in this context is the ASME SA508, used in a variety of reactor facilities, such as pressure vessels, steam generators and pressurisers. The steel is generally given multiple heat

Email address: hp323@cam.ac.uk (H. Pous-Romero)

treatments involving austenitising followed by water quenching, and tempering at temperatures as high as 650°C. The tempering treatment produces a variety of substitutionally–alloyed carbides and can relieve stresses generated by fabrication operations [3].

Within the broad specification of SA508, there is a particular variant, Grade 3, which exhibits better mechanical properties than earlier versions, and is the material of choice for pressure vessels in Gen III plants. There have been many studies of the microstructure obtained after the series of heat treatments described above, with the conclusion that the quenching produces bainite, whereas the tempering leads to the formation of molybdenum rich M₂C precipitates in addition to residual cementite [1, 2, 4–15]. However, there is a lack of information on the austenitising process of SA508 Gr. 3 steels, a key feature of the multiple heat treatments. An understanding of this is important in achieving the optimum austenite grain size, which in turn influences the hardenability and consequently determines the final properties of the steel [16–18].

Austenite grain evolution in SA508 steel has in the past been modelled using a classical relationship of isothermal grain growth [19]:

$$D^n - D_0^n = A \exp\left(\frac{-Q}{RT}\right) t \quad (1)$$

where D_0 and D are the initial and final grain sizes respectively, t is the time at the austenitisation temperature T , n the time exponent, Q is the activation energy for boundary motion, R the universal gas constant and A is a constant depending on the material. The origin of this equation is essentially that the rate of change in grain size depends directly on the amount of grain surface per unit volume that remains within the material. The equation has been widely exploited but it is usually applied empirically, making it less useful when making predictions [17, 20]. Table 1 is a compilation of published models describing the isothermal growth of austenite grains and it is evident that the parameters A , n and Q vary widely in their magnitudes. The initial grain size D_0 is sometimes neglected [18, 20] on the basis that it is smaller than that after coarsening. This assumption is seldom justified, and in any event, the initial grain size will be a function of temperature since the austenite is generated by nucleation and growth during the heating of mixtures of ferrite and cementite.

The purpose of the present work was to develop a physically sound model

Table 1: Summary of empirical models describing austenite grain growth. x_i refers to the concentration in wt% of the element identified by the subscript.

Steel type	Model	n	A	$Q / \text{kJ mol}^{-1}$	Ref.
Rolling C-Mn	$D^n - D_0^n = A \exp\left(\frac{-Q}{RT}\right) t$	10	3.87×10^{32}	400.0 for $T > 1000^\circ\text{C}$	[19]
Rolling C-Mn	"	10	5.02×10^{53}	914.0 for $T < 1000^\circ\text{C}$	[19]
Forged Waspaloy disc	"	3	2×10^{26}		[21]
C-Mn	"	7	1.45×10^{27}		[22]
C-Mn-V	"	10	2.60×10^{28}	437.0	[22]
C-Mn-Ti	"	4.5	4.10×10^{23}		[22]
Micro-alloyed	"	5	1.60×10^{32}	716.9	[23]
Medium C-Nb	"	2.5	1.03×10^{16}	397.7	[20]
C-Mn	"	4.1	1.72×10^{21}	$352.2 + 21.8x_C + 19.9x_{\text{Mn}} + 7.2x_{\text{Cr}} + 7.4x_{\text{Ni}}$	[18]
Low C-Mn	"	2	4.27×10^{12}	278.8	[24]
Low alloy	$D = A \exp\left(\frac{-Q}{RT}\right) t^n$	0.211	76.71×10^3	$89.1 + 3.6x_C + 1.2x_{\text{Ni}} + 1.4x_{\text{Cr}} + 4.0x_{\text{Mo}}$	[17]
Ultrahigh-strength 300M	"	0.17	4.04×10^6	132.0	[25]

for the evolution of the austenite grain structure of SA508 Gr. 3 steel, taking account of the complete heat cycle involved in the generation of the grains.

2. Experimental Procedure

The chemical composition of the steel is given in Table 2. The steel in its as-received state had been subjected to multiple heat treatments: austenitisation between 860 and 880 °C for approximately 12 h, water quenched and tempered between 635 and 655 °C for 10 h. The range in temperatures is due to the thermal gradients in thick samples, which makes the temperature in a particular location uncertain.

Specimens from the as-received condition were reheated at a total of 48 different austenitising conditions at temperatures from 840 °C to 990 °C, and held between $\frac{1}{2}$ h and 13 h. Heat treatments were carried out using a Thermecmaster thermomechanical simulator. Cylindrical samples ($\varnothing 8\text{ mm} \times 12\text{ mm}$) each with a 5 mm wide metallographically-polished flat surface parallel to the long axis were heated under vacuum ($\approx 1\text{ Pa}$) in order to avoid excessive oxidation [26]. The austenite grain boundaries were revealed on the flat surface by the formation of thermal grooves due to the balancing of surface tension forces. The heating and cooling rates used were $\pm 5\text{ }^{\circ}\text{Cs}^{-1}$. The grain sizes were measured using the linear intercept method with data obtained from four different fields of the sample and a total of 72 linear intercept lines.

High-energy X-ray diffraction experiments on as-received specimens were performed at the PETRA III facility in Hamburg. Disk like samples, $\varnothing 8\text{ mm} \times 1\text{ mm}$, were tested in the P02 beam line with a wavelength of 0.20812 \AA , 60 keV and a beam size of $1.2 \times 1.0\text{ mm}$. Transmission diffraction patterns were recorded using a flat 2D solid-state detector, mounted perpendicular to the incident beam behind the sample. The sample to detector distance was 1300 mm to optimise the spatial resolution.

Microstructural features were identified using a range of techniques including transmission electron microscopy. Thin foils for this purpose were prepared by electropolishing with a solution of 5% perchloric acid, 25% glycerol and 70 % ethanol. The voltage, current and temperature during electropolishing were, 37 V, 26 mA and 10 °C respectively.

Thermodynamic calculations were carried out with MTDATA version 4.73 with, PLUS v. 3.02, TFCE v. 1 and SUB SGETE v. 10 as databases.

3. Results and Analysis

The heat treatments given to the as-received steel led to the microstructure illustrated in Fig. 1, consisting of severely tempered bainite platelets, fine needle-shaped molybdenum-rich M₂C carbides, and some coarser cementite particles located at the bainitic ferrite plate boundaries. The structure is important to note because it is the starting condition for the austenitisation experiments described below; previous work has indicated that the initial microstructure can influence the development of austenite during heating [27, 28].

3.1. Austenite grain growth behaviour

Fig. 2 shows the austenite grain growth behaviour as a function of temperature. There is a moderate increase of grain size for temperatures up to 910 °C, e.g. ~13 µm increase after 12 h at 910 °C. However, at 940 °C the size increases significantly, doubling when compared with the lower temperature results. The sudden change in grain growth behaviour observed at 940 °C is typical of cases where a distribution of pinning particles dissolves, permitting a reduction in Zener drag. These particles, if they exist, have not been reported in the nuclear pressure vessel steel of the type studied here in the context of the austenitisation heat treatment (for example in [1, 2, 4–15]).

To investigate further the possibility of pinning particles consistent with the austenitisation temperatures studied, a phase diagram calculation was conducted using MTDATA [29], based on the detailed chemical composition of the steel studied and permitting all the possible phases in the database. The results suggest three possibilities for precipitates stable in the temperature range of interest: AlN, MnS and TiNbCN, Fig. 3, none of which have been observed experimentally. It is significant, however, that it is only the aluminium nitride which exhibits a significant decrease in volume fraction at temperatures around 940 °C, decreasing by a fraction 0.4 over the temperature range 840 to 990 °C. This decrease correlates well with the observed change in growth kinetics and as will be seen later, these calculations led to further verification experiments.

There is clear evidence in low-alloy steels unrelated to the nuclear industry, of a relationship between the austenite grain size and the pinning effect of AlN precipitates [30, 31]. The behaviour reported is similar to that observed here, of grain growth retarded by Zener drag at relatively low temperatures, followed by a large acceleration when the nitride is rendered ineffective by partial or complete dissolution at elevated temperatures. This is in contrast to the gradual

increase in grain coarsening rate in steel without aluminium [31]. The transition between gradual and sudden changes in growth rate is often designated loosely by a *coarsening temperature*, which is a function of the aluminium concentration as illustrated in Fig. 4 [31]. It is interesting that for the present steel which contains 0.0145 wt% aluminium, the coarsening temperature is approximately 940 °C, consistent with the data presented in Fig. 2, although it is emphasised that the available amount of nitrogen must influence the ability to form the nitride, the earlier work supports the contention that the observations of austenite grain growth in SA508 Gr. 3 steel may be explained by particle pinning effects.

Routine X-ray diffraction failed to detect the expected minute quantities of fine AlN < 0.02 wt%, so high-energy X-ray transmission analysis was performed instead, both to enhance resolution and intensity. Fig. 5a shows the intense diffraction peaks of the majority ferrite phase, whereas the weaker but significant contributions from AlN are illustrated in Fig. 5b. The amount of AlN is small but the peaks are fortunately located at positions independent from those due to other phases; the $2\theta = 6.5^\circ$ contribution from AlN is prominent. It is concluded therefore, that AlN precipitates are present in this nuclear pressure vessel steel; some cementite and M₂C precipitates are also noted. Quantitative Rietveld analysis was only possible for cementite which is 2.2 ± 0.5 vol%. Nevertheless, the identification of AlN which remains stable at elevated temperatures where austenite grains are driven to grow, is significant and as far as we are aware, unique.

It is known in the context of other alloys of iron, that AlN precipitation in austenite occurs predominantly at grain boundaries which are heterogeneous nucleation sites and capable of accommodating the considerable volumetric misfit between the AlN and austenite [32–35]. Transmission electron microscopy performed on a sample austenitised at 840 °C for 30 min, clearly revealed grain boundary precipitates in the form of hexagonal cylinders consistent with the hexagonal crystal structure of AlN, Fig. 6. Energy dispersive X-ray analysis confirmed that these particles are rich in aluminium, Fig. 7. These observations together with the thermodynamic calculations serve as a strong indicator that the particles represent AlN which is responsible for Zener pinning the austenite grain boundaries in SA508 Gr. 3 steels.

It is interesting that the austenite grains have an equiaxed shape for all heat treatment temperatures, Fig. 8. At temperatures up to 910 °C, there is a homogeneous distribution in grain sizes, which becomes bimodal and broader at 940 °C, with the abnormalities becoming more marked at long austenitising

times, Fig. 9. Since 940 °C represents a temperature where the role of AlN is diminishing, the bimodal size distribution may reflect localised reductions in pinning forces associated with the heterogeneous dissolution of the nitride.

3.2. Modelling austenite grain growth

It is generally accepted that the boundary migration velocity (ν) is proportional to the driving force [36], an approximation [37] justified at the rather small driving forces involved in grain growth:

$$\nu = M \Delta\mu \quad \text{where} \quad \Delta\mu = C_1 \left(\frac{1}{D} - \frac{1}{D_{Lim}} \right) \quad (2)$$

where M is the boundary mobility, $\Delta\mu$ the driving free energy per unit volume for boundary migration and C_1 is a constant which contains the interfacial energy per unit area. D_{Lim} is a grain size limited by particle pinning, representing the point where the driving force for growth equals the opposing pinning force. If the boundary velocity is written as dD/dt , and the temperature dependence of the mobility expanded as $M \propto \exp\left(\frac{-Q}{RT}\right)$, then it follows that [38]:

$$\frac{dD}{dt} = A \exp\left(\frac{-Q}{RT}\right) \left[\frac{1}{D} - \frac{1}{D_{Lim}} \right] \quad (3)$$

where t the time, T the temperature, Q an activation energy for grain growth, R the universal gas constant and A is a constant which includes C_1 . On integration this gives [38]:

$$\begin{aligned} -DD_{Lim} - D_{Lim}^2 \ln\left(1 - \frac{D}{D_{Lim}}\right) + D_0 D_{Lim} + D_{Lim}^2 \ln\left(1 - \frac{D_0}{D_{Lim}}\right) \\ = A \exp\left(\frac{-Q}{RT}\right) t \end{aligned} \quad (4)$$

where D_0 is the initial grain size which must be known as a function of temperature; a common approximation is to set it to zero, but this may not be reasonable for the present work since nuclear pressure vessels are large components which take time to reach the desired austenitisation temperature. To resolve this, we recognise that the very first austenite grain size is defined when the steel becomes fully austenitic at a temperature Ac_3 , and that there may be subsequent grain growth during heating to the isothermal austenitisation temperature. Assuming a continuous heating curve, it can be expressed as a sum

of short time isothermal holding as is shown in Fig. 10.

Growth during continuous heating between the Ac_3 and heat treatment temperature can be considered as a series of n isothermal steps with each successive step at a slightly greater temperature. The definition of $D_0 \geq D_{\text{Ac}3}$ is then the size at the point where the isothermal austenitisation temperature is reached:

$$\begin{aligned} -D_0 D_{\text{Lim}} - D_{\text{Lim}}^2 \ln \left(1 - \frac{D_0}{D_{\text{Lim}}} \right) + D_{\text{Ac}3} D_{\text{Lim}} + D_{\text{Lim}}^2 \ln \left(1 - \frac{D_{\text{Ac}3}}{D_{\text{Lim}}} \right) \\ = \sum_{i=1}^n A \exp \left(\frac{-Q}{RT_i} \right) \Delta t_i \end{aligned} \quad (5)$$

Since the heating rate can be expressed as: $\alpha = \Delta T_i / \Delta t_i$, Eq. 5 can be rearranged as a function of the heating rate over the range of temperatures from Ac_3 to the holding temperature (T):

$$\begin{aligned} -DD_{\text{Lim}} - D_{\text{Lim}}^2 \ln \left(1 - \frac{D}{D_{\text{Lim}}} \right) + D_{\text{Ac}3} D_{\text{Lim}} + D_{\text{Lim}}^2 \ln \left(1 - \frac{D_{\text{Ac}3}}{D_{\text{Lim}}} \right) \\ = A \exp \left(\frac{-Q}{RT} \right) t + \frac{A}{\alpha} \int_{\text{Ac}3}^T \exp \left(\frac{-Q}{RT} \right) dT \end{aligned} \quad (6)$$

It is necessary to know the limiting grain size as a function of temperature in order to exploit this equation, and D_{Lim} is not constant since the fraction of AlN will change with temperature. Therefore, D_{Lim} was assumed to be the largest grain size measured at each temperature plus the error in the grain size measurement; e.g. the austenite grain size measured at 940 °C after 12 h is $54 \pm 3 \mu\text{m}$, so $D_{\text{Lim}} = 57 \mu\text{m}$. The value for 990 °C was not included since the grain size did not seem to reach a limiting value in that case (Fig. 2).

To reveal $D_{\text{Ac}3}$ by thermal etching, samples were heated under vacuum to the Ac_3 temperature and then, rapidly-cooled to room temperature. Dilatometric experiments have been used to identify the Ac temperatures. The experimentally established Ac_1 and Ac_3 temperatures are 760 and 823 °C, respectively. The grain size $D_{\text{Ac}3}$ was determined to be $3 \pm 0.5 \mu\text{m}$.

The two unknowns in Eq. 6 are the activation energy Q and the constant A ; the latter can be deduced by rearranging the equation so as to permit linear

regression, as a function of an assumed value of Q :

$$\begin{aligned} & \overbrace{\ln \left[-DD_{Lim} - D_{Lim}^2 \ln \left(1 - \frac{D}{D_{Lim}} \right) + D_{Ac3} D_{Lim} + D_{Lim}^2 \ln \left(1 - \frac{D_{Ac3}}{D_{Lim}} \right) \right]}^Y \\ & = \ln A + \overbrace{\ln \left[\exp \left(\frac{-Q}{RT} \right) t + \frac{1}{\alpha} \int_{Ac3}^T \exp \left(\frac{-Q}{RT} \right) dT \right]}^X \end{aligned} \quad (7)$$

The activation energy can then be fixed by the value of Q which gives the maximum correlation between X and Y, Fig. 11. By applying this methodology the calculated value of Q is 310 kJ mol^{-1} ; the physical significance of this is considered next.

4. Activation energy for grain growth

In theory, the activation energy for the transfer of atoms across a general grain boundary should be about half that for self-diffusion [37]. The activation energy for iron diffusion in austenite is 286 kJ mol^{-1} [39] so that the expected Q should be about 143 kJ mol^{-1} , unlike the 310 kJ mol^{-1} deduced above. Large activation energies are also reported in many studies, as listed in Table 1. There is a dearth of explanations in the past, but one possibility is that there is a non-linear relationship between driving force and boundary velocity [18, 40], but as stated previously, the driving force for grain growth is very small, much smaller than for example in solid-state phase transformations in steels, where the linear relationship applies well, for example [41]. It was felt instead that the usual analysis methods do not account sufficiently for uncertainties, which may lead to over-fitting of the experimental data.

The over-fitting problem was assessed by introducing the variable X as input and Y as output (based on a particular Q) as defined in Eq. 7, into a Bayesian neural network [42–44] with a single hidden unit in order to emulate linear regression. The method provides measures of over-fitting by using only half of the randomly chosen training data to create the model, and then testing the model on the unseen test data. The error in predicting the test data should be similar to that obtained for the training data in order to conclude optimum fitting. Indeed, both the training and test errors should lie within the maximum and minimum bounds of the experimental error in the grain size measurement. Judging from Fig. 12, it is evident that the value of $Q = 190 \text{ kJ mol}^{-1}$ represents

an optimal fit to the experimental data, with either higher or lower values violating the criteria described. The conclusion must therefore be that very large values of Q reported in the literature are not justified by the experimental errors in the grain size data, and that the 190 kJ mol^{-1} is consistent with the theory that the activation energy for grain boundary motion should be about half that for self-diffusion. The final grain growth equation for the steel studied here therefore becomes:

$$\begin{aligned} & -DD_{Lim} - D_{Lim}^2 \ln \left(1 - \frac{D}{D_{Lim}} \right) + D_{Ac3} D_{Lim} + D_{Lim}^2 \ln \left(1 - \frac{D_{Ac3}}{D_{Lim}} \right) \\ & = \exp \left(1.324 \ln \left[\exp \left(\frac{-Q}{RT} \right) t + \frac{1}{\alpha} \int_{Ac3}^T \exp \left(\frac{-Q}{RT} \right) dT \right] + 19.125 \right) \end{aligned} \quad (8)$$

where the grain sizes are in μm , the activation energy for grain growth $Q=190,000\text{ J mol}^{-1}$, T is in Kelvin, t in seconds and α is the heating rate in K s^{-1} . The comparison between experimental data and this equation is illustrated in Fig. 13, showing reasonable agreement with a standard error of $4\text{ }\mu\text{m}$.

Given that the theoretical approach leads to a physically meaningful Q , accounts for the initial grain size and the heating rate to the isothermal holding temperature, test were designed to assess the ability of the model to generalise on unseen data. Grain sizes were measured for five new austenitising conditions; Table 3 shows that reasonable agreement is obtained between the measurements and predictions.

5. Conclusions

Austenite grain growth in a nuclear pressure vessel steel, SA508 Gr. 3, has been studied with the aim of deriving a physically reasonable expression which generalises well. The essential conclusions can be summarised as follows:

1. The kinetics of the isothermal growth of austenite grains can be categorised into two temperature regimes, one in which the boundaries experience a pinning force due to precipitates so that the grain size rapidly reaches a limiting value. In contrast, at higher temperatures where the precipitates are expected to dissolve, not only is the rate of grain growth dramatically increased, but also does not reach a limiting value within the time scale of the experiments reported here.
2. It has been established using thermodynamic calculations, high-energy X-ray diffraction, transmission electron microscopy and microanalysis, that the pinning particles at the temperatures of interest are aluminium nitrides.
3. The standard theory for grain growth has been adapted to account for the initial grain size generated as the steel reaches its fully austenitic state, and for the evolution of this size as the sample is heated continuously to the isothermal annealing temperature.
4. It is demonstrated that the activation energy for grain growth is, as expected, about half that for the self-diffusion of iron in austenite, once the data are interpreted to avoid over-fitting. The activation energy is thus found to be about 190 kJ mol^{-1} , a value much smaller than most reported data on nuclear pressure vessel steels.

Acknowledgments: The authors are grateful to Rolls-Royce plc for sponsoring this work. Discussions with staff at Sheffield Forgemasters are also appreciated.

- [1] S. Kim, Y. Im, S. Lee, H. Lee, Y. J. Oh, and J. H. Hong. Effects of alloying elements on mechanical and fracture properties of base metals and simulated HAZ of SA508 steels. *Metallurgical and Materials Transactions A*, 32A:903–911, 2001.
- [2] S. Lee, S. Kim, B. Hwang, B. S. Lee, and C. G. Lee. Effect of carbide distribution on the fracture toughness in the transition temperature region of an SA508 steel. *Acta Materialia*, 50:5755–4762, 2002.
- [3] H.-H. Jin, C. Shin, D. H. Kim, K. H. Oh, and J. Kwon. Evolution of needle shaped carbide in SA508 Gr3 steel. *ISIJ International*, 48:1810–1812, 2008.
- [4] B.S. Lee, J.H. Hong, W.J. Yang, M.Y. Huh, and S.H. Chi. Master curve characterization of the fracture toughness in unirradiated and irradiated RPV steels using full- and 1/3-size pre-cracked Charpy specimens. *International Journal of Pressure Vessels and Piping*, 77:599–604, 2000.
- [5] X.Q. Wu and I.S. Kim. Effects of strain rate and temperature on tensile behavior of hydrogen-charged SA508 Cl.3 pressure vessel steel. *Materials Science and Engineering A*, 348:309–318, 2003.
- [6] S.H. Chi and G.E. Lucas. Differences in mechanical properties and microstructure of SA508 CL. 3 reactor pressure vessel steels manufactured by different steel refining process. *Transactions of the 15th International Conference on Structural Mechanics in Reactor Technology*, pages 223–230, 1999.
- [7] B. S. Lee, M. C. Kim, J. H. Yoon, and J. H. Hong. Characterization of high strength and high toughness Ni-Mo-Cr low alloy steels for nuclear application. *International Journal of Pressure Vessels and Piping*, pages 74–80, 2010.
- [8] Y. S. Ahn, H. D. Kim, T. S. Byun, Y. J. Oh, G. M. Kim, and J. H. Hong. Application of intercritical heat treatment to improve toughness of SA508 Cl.3 reactor pressure vessel steel. *Nuclear Engineering and Design*, 194:161–177, 1999.
- [9] T. S. Byun, J. H. Hong, F. M. Haggag, K. Farrell, and E. H. Lee. Measurement of through-the-thickness variations of mechanical properties in SA508

Gr.3 pressure vessel steels using ball indentation test technique. *International Journal of Pressure Vessels and Piping*, 74:231–238, 1997.

- [10] M. S. Garcia-Redondo, M. L. Castano-Marin, and D. Gomez-Briceno. Comportamiento del acero de baja aleacion SA508 y del acero al carbono A410b en las condiciones de operacion y parada del circuito primario de los reactores de agua ligera tipo PWR. *Revista de Metalurgia Madrid*, 36:88–99, 2000.
- [11] Y. R. Im, Y. J. Oh, B. J. Lee, J. H. Hong, and H. C. Lee. Effects of carbide precipitation on the strength and charpy impact properties of low carbon Mn-Ni-Mo bainitic steels. *Journal of Nuclear Materials*, 297:138–148, 2001.
- [12] K. Suzuki, I. Kurihara, Sasaki, Y. Koyoma, and Y. Tanakaca. Application of high strength MnMoNi steel to pressure vessels for nuclear power plant. *Nuclear Engineering and Design*, 206:261–278, 2001.
- [13] S. Kim, S. Lee, Y. R. IM, S. J. Kim H. C. Lee, and J. H. Hong. Effects of alloying elements on fracture toughness in the transition temperature region of base metals and simulated heat-affected zones of Mn-Mo-Ni low alloy steels. *Metallurgical and Materials Transactions*, 35A:2027–2037, 2004.
- [14] Y.R. Im, B.J. Lee, Y. J. Oh, J.H. Hong, and H.C. Lee. Effect of microstructure on the cleavage fracture strength of low carbon Mn-Ni-Mo bainitic steels. *Journal of Nuclear Materials*, 324:33–40, 2004.
- [15] K. D. Haverkamp, K. Forch, K. H. Piehl, and W. Witte. Effect of heat treatment and precipitation state in toughness of heavy section Mn-Mo-Ni-steel for nuclear power plants components. *Nuclear Engineering and Design*, 81:207–217, 1984.
- [16] L. M. Fu, H. R. Wang, W. Wang, and A. D .Shan. Austenite grain growth prediction coupling with drag and pinning effects in low carbon Nb microalloyed steels. *Materials Science and Technology*, 27(6):996–1001, 2011.
- [17] S. Lee and Y. Lee. Prediction of austenite grain growth during austenitization of low alloy steels. *Materials and Design*, 29:1840–1844, 2008.
- [18] S. Uhm, J. Moon, C. Lee, J. Yoon, and B. Lee. Prediction model for the austenite grain size in the coarse grained heat affected zone of Fe-C-Mn steels: Considering the effect of initial grain size on isothermal growth

- behavior. *Iron and Steel Institute of Japan International*, 44(7):1230–1237, 2004.
- [19] C. M. Sellars and J. A. Whiteman. Recrystallization and grain growth in hot rolling. *Metal Science*, pages 187–194, 1979.
 - [20] Y. Zhao, J. Shi, W. Cao, M. Wang, and G. Xie. Kinetics of austenite grain growth in medium-carbon niobium-bearing steel. *Applied Physics and Engineering*, 12:171–176, 2011.
 - [21] G. Shen, J. Rollins, and D. Furrer. Microstructure modeling of forged waspaloy discs. In R. D. Kissinger, D. J. Deye, and D. A. Woodford, editors, *Superalloys 1996*. The Minerals, Metals and Materials Society, 1996.
 - [22] P. D. Hodgson and R. K. Gibbs. A mathematical model to predict the mechanical properties of hot rolled C-Mn and microalloyed steels. *Iron and Steel Institute of Japan International*, 32(12):1329–1338, 1992.
 - [23] J. Wang, J. Chen, Z. Zhao, and X. Y. Ruan. Modeling of microstructural evolution in microalloyed steel during hot forging process. *Acta Materialia*, 19(4):279–286, 2006.
 - [24] S. Nanba, M. Kitamura, M. Shimada, M. Katsumata, T. Inoue, H. Ima-mura, Y. Maeda, and S. Hattori. Prediction of microstructure distribution in the through-thicknesss direction during and after hot rolling in carbon steels. *Iron and Steel Institute of Japan International*, 32(3):377–386, 1992.
 - [25] S. S. Zhang, M. Q. Li, Y. G. Liu, J. Luo, and T. Q. Liu. The growth behavior of austenite grain in the heating process of 300M steel. *Materials Science and Engineering A*, 528:4967–4972, 2011.
 - [26] C. Garcia de Andrés, M. J. Bartolomé, C. Capdevila, D. San Martín, F. G Caballero, and V. Lopez. Metallographic techniques for the determination of the austenite grain size in medium-carbon microalloyed steel. *Materials Characterization*, 46:389–398, 2001.
 - [27] L. Gavard, H. K. D. H. Bhadeshia, D. J. C. MacKay, and S. Suzuki. Bayesian neural network model for austenite formation in steels. *Materials Science and Technology*, 12:453–463, 1996.
 - [28] F. G. Caballero, C. Capdevila, and C. Garcia de Andres. Modelling of kinetics and dilatometric behaviour of austenite formation in a low-carbon

- steel with a ferrite plus pearlite initial microstructure. *Journal of Materials Science*, 37:3533–3540, 2002.
- [29] NPL. MTDATA. Software, National Physical Laboratory, Teddington, U.K., 2006.
- [30] M. Militzer, A. Gumelli, E. B. Hawbolt, and T. R. Meadowcroft. Austenite grain growth kinetics in a-killed plain carbon steels. *Metallurgical and Materials Transactions A*, 27A:3399–3496, 1996.
- [31] T. Gladman and F. B. Pickering. Grain coarsening of austenite. *Journal of the Iron and Steel Institute*, 205:653–664, 1967.
- [32] R. Radis and E. Kozeschnik. Kinetics of AlN precipitation in microalloyed steel. *Modelling and Simulation in Materials Science and Engineering*, 18:1–16, 2010.
- [33] F. G. Wilson and T. Gladman. Aluminun nitride in steel. *International Materials Reviews*, 33:211–283, 1988.
- [34] R. J. Bruls, H. T. Hintzen, G. de With, R. Metselaar, and J. C. van Miltenburg. The temperature dependence of the Grueneisen parameters of MgSiN₂, AlN and B-Si₃N₄. *Journal of Physics and Chemistry of Solids*, 62:783–792, 2001.
- [35] L. T. Lu, K. Shiozawa, Y. Morii, and S. Nishino. Fatigue fracture process of a high-carbon-chromium bearing steel in ultra-long life regime. *Acta Metallurgica Sinica*, 41:1066–1072, 2005.
- [36] J. W. Martin, R. D. Doherty, and B. Cantor. *Stability of microstructure in metallic systems*. Cambridge University Press, Cambridge, U. K., 2 edition, 1997.
- [37] J. W. Christian. *Theory of Transformations in Metal and Alloys, Part I*. Pergamon Press, Oxford, U. K., 3 edition, 2003.
- [38] I. Andresen and O. Grong. Analytical modelling of grain growth in metals and alloys in the presence of growing and dissolving precipitates-I. Normal grain growth. *Acta Metallurgica et Materialia*, 43:2673–1688, 1995.
- [39] J. Fridberg, L.-E. Torndähł, and M. Hillert. Diffusion in iron. *Jernkontorets Annaler*, 153:263–276, 1969.

- [40] P. A. Manohar, D. P. Dunee, T. Chandra, and C. R. Killmore. Grain growth predictions in microalloyed steels. *Iron and Steel Institute of Japan International*, 36:194–200, 1996.
- [41] G. P. Krielaart, J. Sietsma, and S. van der Zwaag. Ferrite formation in Fe-C alloys during austenite decomposition under non equilibrium interface conditions. *Materials Science & Engineering A*, 237:216–223, 1997.
- [42] D. J. C. MacKay. Practical Bayesian framework of backpropagation networks. *Neural Computation*, 4:448–472, 1992.
- [43] D. J. C. MacKay. Bayesian interpolation. *Neural Computation*, 4:415–447, 1992.
- [44] H. K. D. H. Bhadeshia. Neural networks in materials science. *ISIJ International*, 39:966–979, 1999.

List of Figures

1	Transmission electron micrograph of as-received steel.	18
2	Isothermal grain growth behaviour of austenite.	18
3	Equilibrium phase diagram calculated by MTDATA at the austenitising temperatures for the as-received composition.	19
4	Effect of Al content on grain coarsening temperature. The nitrogen content for the data ranges from 0.009 – 0.016 wt%. Data from [31].	19
5	Synchrotron high-energy X-ray spectra for as-received SA508 Gr. 3 steel. a) Full spectra. b) Magnified area showing AlN, M ₂ C and cementite peaks.	20
6	STEM micrograph of SA508 Gr. 3 steel austenitised at 840 °C for 30 min, showing grain boundary precipitates.	21
7	EDX analysis of grain boundary precipitates.	22
8	Effects of austenitising condition in grain size of SA508 Gr 3. . .	23
9	Grain size distribution for SA508 Gr. 3 steel at different austenitising conditions.	24
10	Continuous heating curve expressed by a sum of isothermal holdings.	24
11	Variation of correlation with different values of activation energy for grain growth, Q . X and Y as defined in Eq. ???. Dotted lines represent the error between the linear regression line and the data.	25
12	Effect of variation of activation energy for grain growth in the test and training errors. Dotted lines represent the maximum, average and minimum experimental errors from the grain size measurements.	26
13	Comparison of calculated and measured austenite grain sizes . .	26

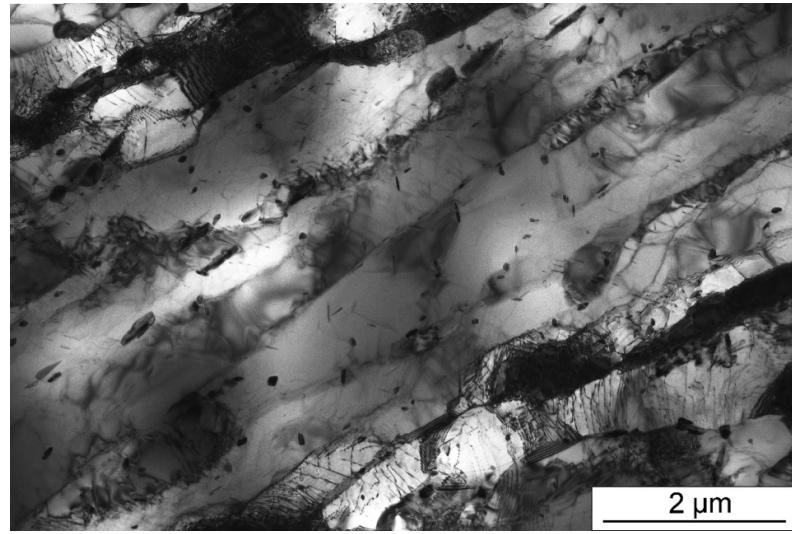


Figure 1: Transmission electron micrograph of as-received steel.

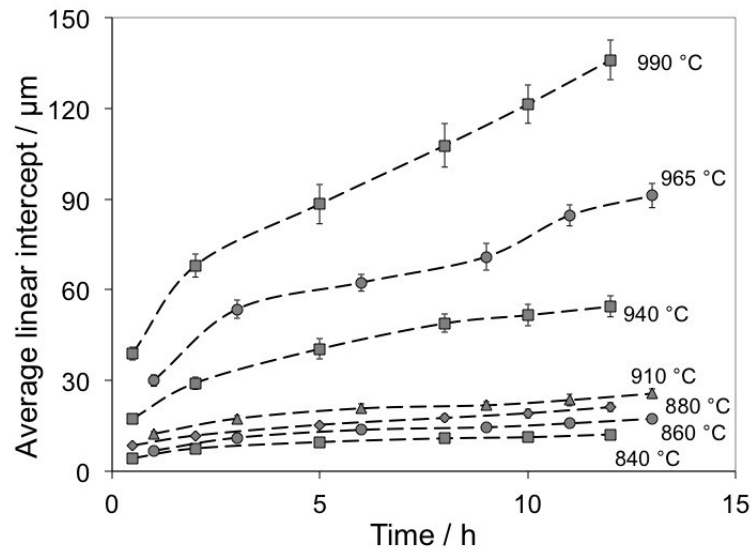


Figure 2: Isothermal grain growth behaviour of austenite.

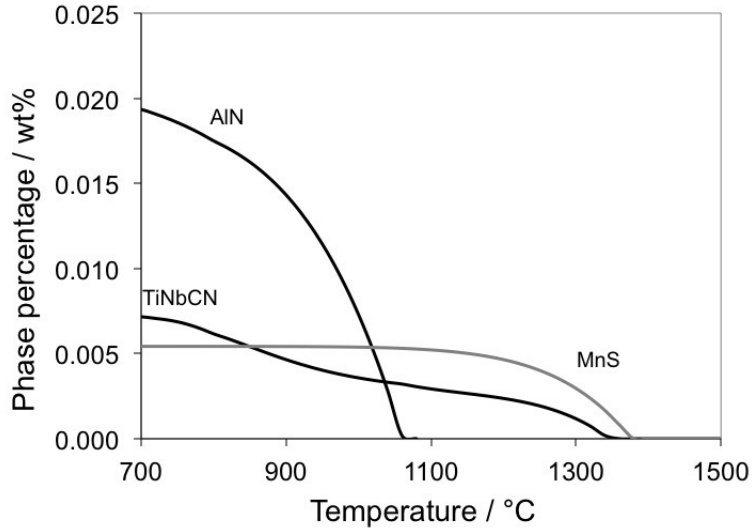


Figure 3: Equilibrium phase diagram calculated by MTDATA at the austenitising temperatures for the as-received composition.

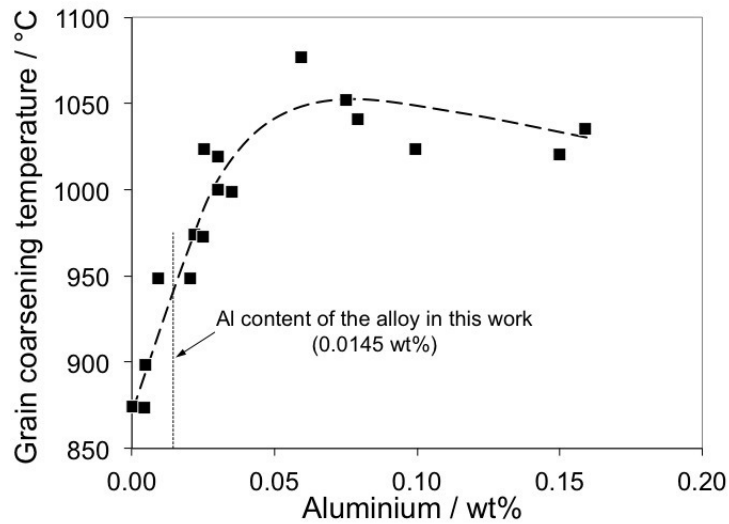


Figure 4: Effect of Al content on grain coarsening temperature. The nitrogen content for the data ranges from 0.009 – 0.016 wt%. Data from [31].

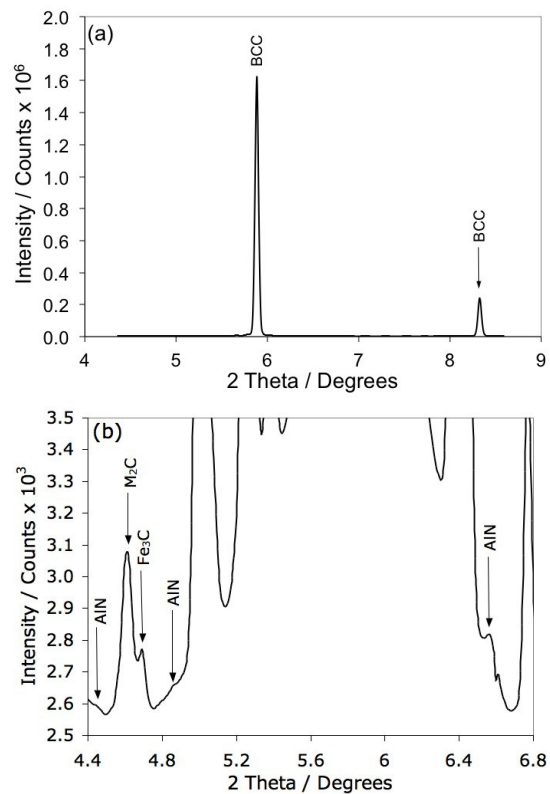


Figure 5: Synchrotron high-energy X-ray spectra for as-received SA508 Gr. 3 steel. a) Full spectra. b) Magnified area showing AlN, M₂C and cementite peaks.

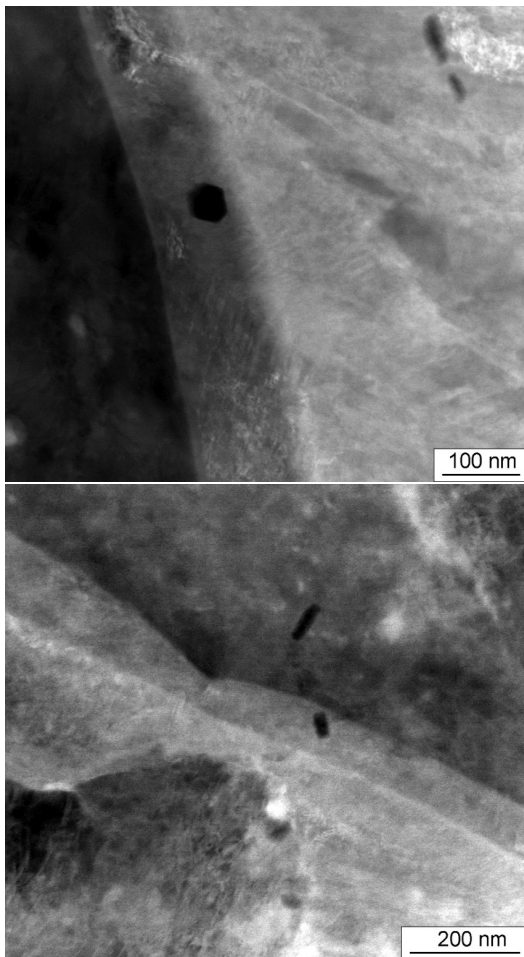


Figure 6: STEM micrograph of SA508 Gr. 3 steel austenitised at 840 °C for 30 min, showing grain boundary precipitates.

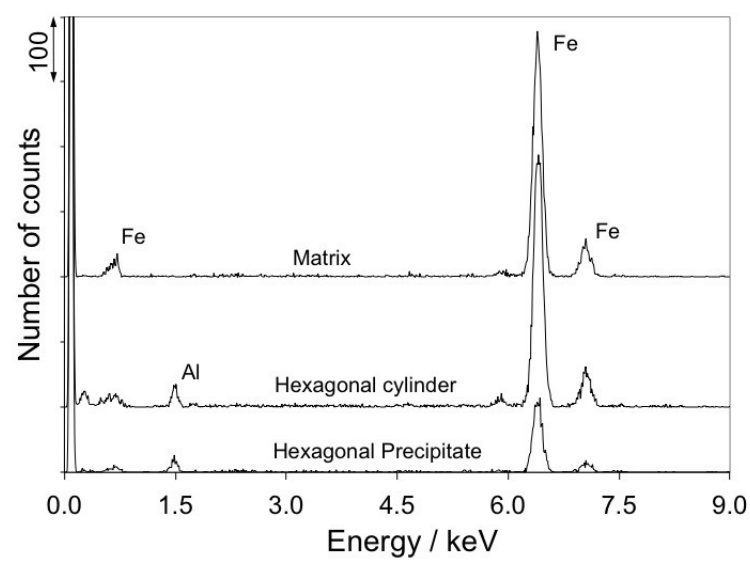


Figure 7: EDX analysis of grain boundary precipitates.

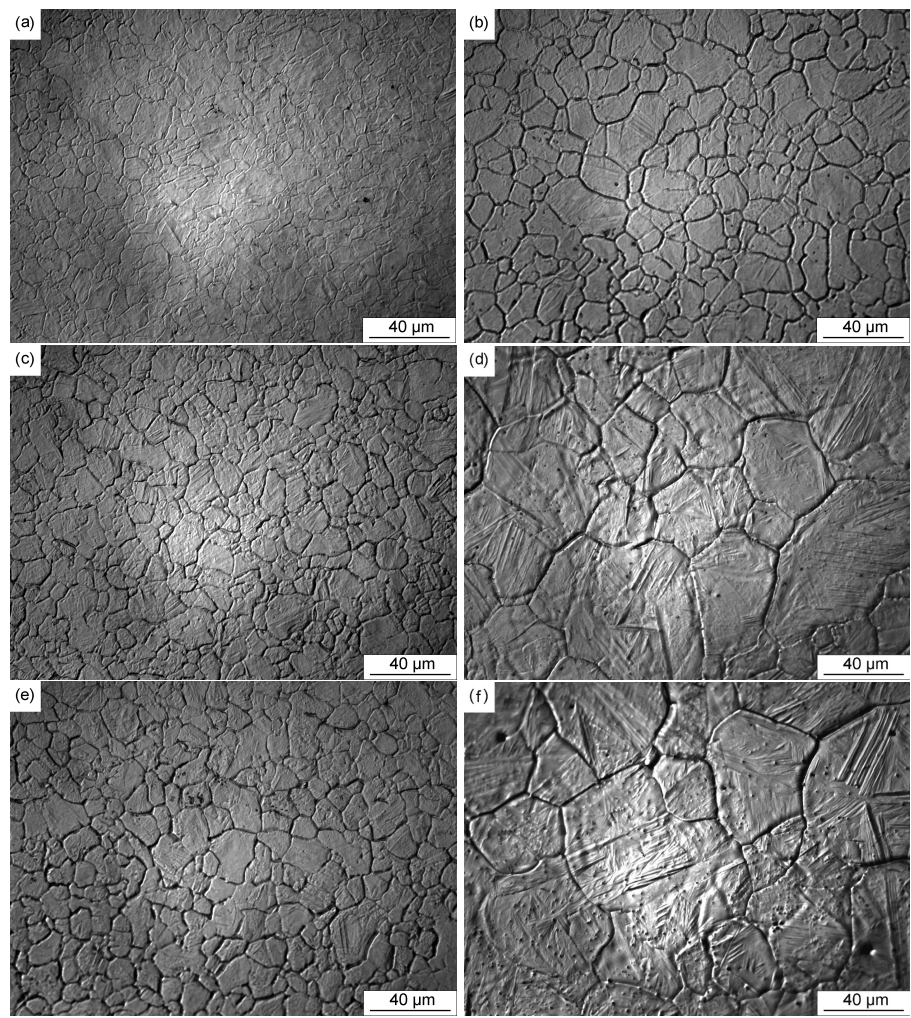


Figure 8: Effects of austenitising condition in grain size of SA508 Gr 3 steel. a) 840 °C for 30 min; b) 940 °C for 30 min; c) 840 °C for 5 h; d) 940 °C for 5 h; e) 840 °C for 12 h; f) 940 °C for 12 h

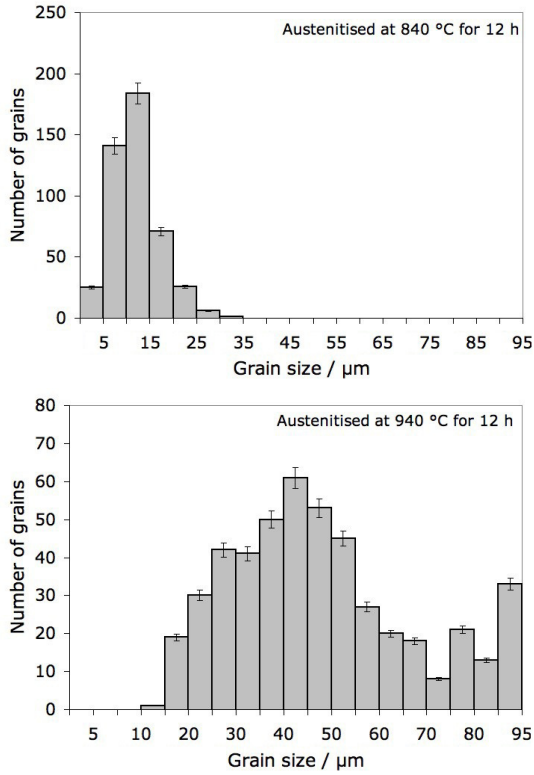


Figure 9: Grain size distribution for SA508 Gr. 3 steel at different austenitising conditions.

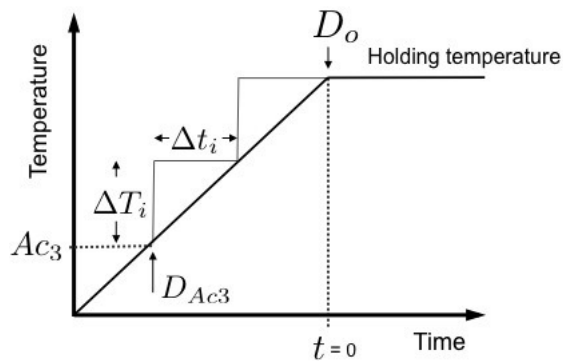


Figure 10: Continuous heating curve expressed by a sum of isothermal holdings. Where D_{Ac3} is the austenite grain size at Ac_3 , D_o the initial austenite grain size at holding temperature, Δt_i time interval and ΔT_i is temperature difference.

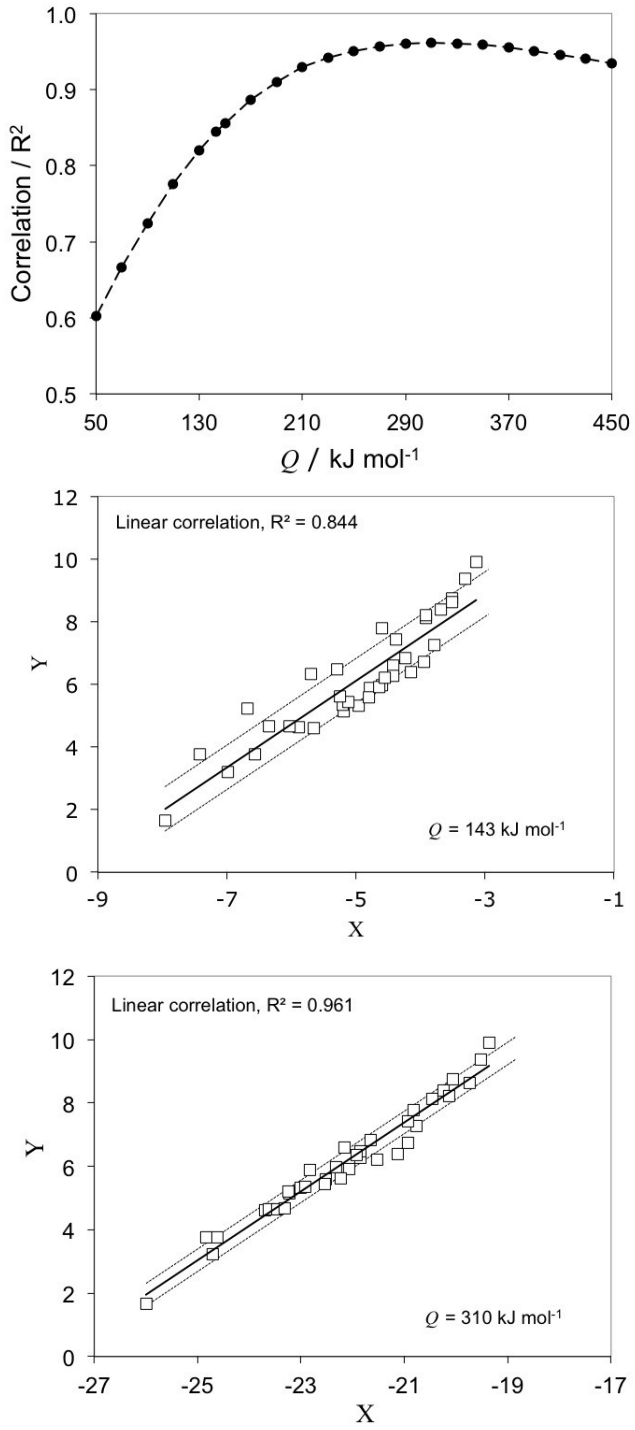


Figure 11: Variation of correlation with different values of activation energy for grain growth, Q . X and Y as defined in Eq. 7. Dotted lines represent the error between the linear regression line and the data.

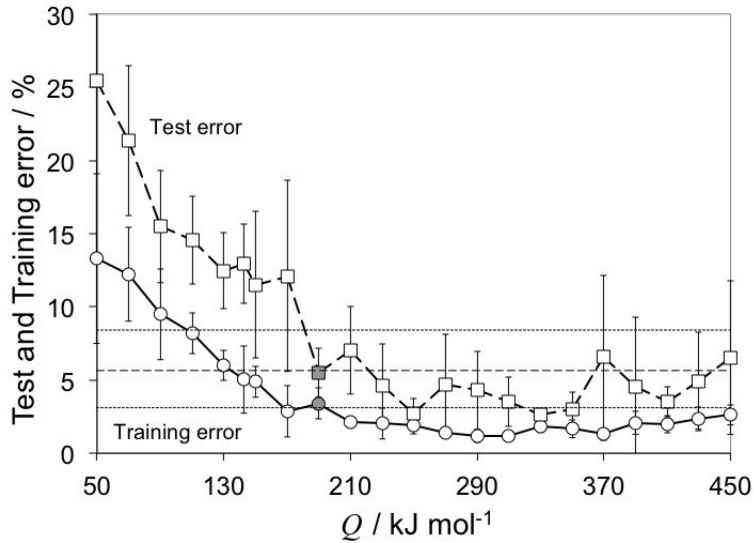


Figure 12: Effect of variation of activation energy for grain growth in the test and training errors. Dotted lines represent the maximum, average and minimum experimental errors from the grain size measurements.

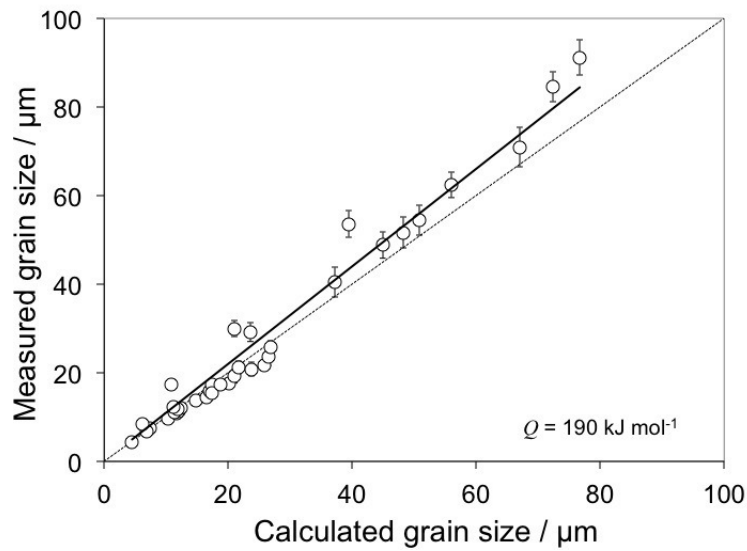


Figure 13: Comparison of calculated and measured austenite grain sizes.

List of Tables

1	Summary of empirical models describing austenite grain growth. x_i refers to the concentration in wt% of the element identified by the subscript.	3
2	Chemical composition of as-received SA508 Gr. 3 steel (wt%). . .	28
3	Measured and calculated austenite grain sizes.	28

Table 2: Chemical composition of as-received SA508 Gr. 3 steel (wt%).

C	Mn	Ni	Mo	Cr	Si	Cu	P	S
0.17	1.315	0.785	0.53	0.27	0.22	0.04	0.004	0.002
Co	Al	Nb	Ti	Sb	As	Sn	N	H
0.01	0.0145	0.004	0.002	0.002	0.005	0.006	0.007	0.65 (ppm)

Table 3: Measured and calculated austenite grain sizes.

Test	Temperature / °C	Time / h	Measured grain size / μm	Calculated grain size / μm
<i>a</i>	925	1	18 ± 1	14 ± 4
<i>b</i>	925	3	25 ± 2	25 ± 4
<i>c</i>	925	5	32 ± 2	32 ± 4
<i>d</i>	925	13	48 ± 4	45 ± 4
<i>e</i>	1200	48	221 ± 19	240 ± 4